

# ULRR

## Acoustic analysis of vortex-based cavitation devices: inception and extent of cavitation

Item Type	Article
Authors	Ranade, Nanda V.;Sarvothaman, Varaha;Ranade, Vivek
Citation	Industrial & Engineering Chemistry Research, 2021, 60 (22), pp. 8255-8268
Publisher	American Chemical Society
Download date	2026-04-17 22:37:38
Item License	<a href="https://creativecommons.org/licenses/by-nc-sa/4.0/">https://creativecommons.org/licenses/by-nc-sa/4.0/</a>
Link to Item	<a href="https://doi.org/10.34961/researchrepository-ul.26190551">https://doi.org/10.34961/researchrepository-ul.26190551</a>

# Acoustic Analysis of Vortex-based Cavitation Devices: Inception and extent of cavitation

Nanda V. Ranade<sup>1</sup>, Varaha Sarvothaman<sup>2</sup>, and Vivek V. Ranade<sup>2,3\*</sup>

<sup>1</sup>Hollyheath, 14 Derryvolgie Avenue, Belfast BT9 6FB, UK

Multiphase Reactors & Intensification Group (mRING)

<sup>2</sup>School of Chemistry and Chemical Engineering  
Queen's University Belfast, Belfast BT9 5AG, UK

<sup>3</sup>Bernal Institute, University of Limerick  
Limerick V94 T9PX, Ireland

\* Author to whom correspondence should be addressed

Email: [V.Ranade@qub.ac.uk](mailto:V.Ranade@qub.ac.uk), [Vivek.Ranade@ul.ie](mailto:Vivek.Ranade@ul.ie)

## Abstract

Hydrodynamic cavitation (HC) is a process of generation, growth and collapse of gas/vapour filled cavities leading to intense shear and localised hot spots. It is essential to identify the inception and extent of cavitation for ensuring appropriate operation of HC devices and processes. In this work, we demonstrate for the first time, usefulness of acoustic data acquired using an everyday mobile phone for characterising inception and extent of cavitation. Acoustic data from vortex based cavitation devices for a range of operating pressure drop (0 – 390 kPa) was obtained. Systematic methodology for identifying relevant acoustic features is presented. 'Audio' and 'DSP' Toolboxes of MATLAB were used for processing acoustic data. Three specific trends of extracted features with respect to flow rate/ pressure drop across HC device were observed. All the three trends clearly identified inception of cavitation between 50 to 80 kPa pressure drop across the HC device. An attempt is made to connect features extracted from acoustic signals with the extent of cavitation in terms of per-pass performance of HC device. The 'flatness' was found to capture influence of HC device scale on performance (in other words, extent of cavitation) reasonably well. The methodology is quite general and will be applicable for any cavitation device. The presented results will be useful for on-line identification of inception and extent of hydrodynamic cavitation.

**Key words:** Hydrodynamic cavitation, acoustic signals, spectrogram, audio feature extraction.

## 1. Introduction

Hydrodynamic cavitation (HC) is the formation, growth and subsequent collapse of gas/vapour filled cavities in a flowing liquid. The collapse of these cavities leads to intense shear and generation of hydroxyl radicals, which can be harnessed for realising desired physicochemical transformations and industrially relevant applications<sup>1-6</sup>. Inception of HC occurs when the low pressure generated in a cavitation device approaches vapour pressure of liquid. At very low flow rates through a cavitation device (that is at low operating pressure drop conditions across cavitation device), the lowest pressure generated may not be sufficiently low to generate cavities. As the flow rate increases, at a certain point, the lowest pressure generated within the system may approach vapour pressure leading to an inception of cavitation. It is important to identify this condition for ensuring appropriate operation of HC devices and processes.

At the inception of cavitation, cavities emerge from single-phase flow and turn it into a multiphase flow. The generated cavities collapse when they travel to high-pressure regions and experience turbulent pressure fluctuations. The collapse of cavities leads to significant noise<sup>7</sup>, shear<sup>4,7</sup> and localised hot spots<sup>9</sup>. The simplest method to detect cavitation is a visual method provided that the cavitation devices and associated piping are transparent<sup>10,11</sup>. More sophisticated visual techniques such as high-speed imaging<sup>12</sup>, light scattering methods<sup>13</sup> and particle imaging velocimetry<sup>14</sup> have also been used. Visual methods (either manual or with cameras) are not applicable for opaque cavitation devices. Other methods for detecting inception of cavitation rely on quantifying the effects of cavitation. Various chemical methods (usually termed as dosimetry methods) use radical scavengers to quantify generated radicals (indirectly by analysing products of reaction between selected scavenger and OH radicals) and therefore can be used for detecting cavitation. The commonly used scavengers for cavitation are salicylic acid<sup>15</sup>, terephthalic acid<sup>16</sup>, potassium iodide<sup>11</sup> and coumarin<sup>17</sup>. Though dosimetry based methods are useful for identifying inception and extent of cavitation, these require expensive analytical equipment and are difficult to implement for on-line identification.

It is also possible to detect the cavitation inception by acoustic means<sup>18,19</sup>. The identification of inception via acoustic methods is of interest to maritime industries<sup>20</sup> as well as process industries using HC devices<sup>21,22</sup>. These acoustic methods rely on the increased sound levels generated by the collapsing cavities. Several studies have described cavitation noise: for example, a tip vortex was reported as a 'singing vortex'<sup>23</sup> because of the cavitation noise or the cavitation noise from an orifice was described as pebbles being rolled through the device<sup>24</sup>. A hydrophone type of instrument is commonly used for the acquisition of noise<sup>19,25</sup>. Hydrophones are especially useful for underwater acquisition given the

requirement of acquisition in propellers and turbines<sup>20</sup>. Different data processing techniques on the time and frequency spectra are used to analyse the cavitation noise: for example, the counting of number of peaks larger than certain threshold<sup>26-28</sup> and Fast Fourier Transform spectra<sup>7,20-22,29,30</sup> are used to identify the inception condition.

Wang et al.<sup>31</sup> have used hydrophone for acquiring pressure signals for characterising cavitation in different Jet Pump Cavitation Reactors (JPCR). Spectrograms within the frequency range 0.1 to 100 kHz for different flow ratios in a JPCR are reported. Amplitude changes in spectrogram are noted in the range 200 to 4000 Hz due to cavitation at different flow ratios. A detailed analysis of extracted features is however missing. Tabrizi and Wu<sup>32</sup> have investigated noise of a cavitating orifice using CFD simulations and fw-h formulations to gain insight into acoustic conditions. They have reported comparison between spectra of developed cavitation and super cavitation with qualitative description of the spectra. Increase in amplitude with super cavitation is also mentioned. However, method of quantifying extent of cavitation is not discussed. Park and Seong<sup>33</sup> have compared power spectral densities for developed, incipient and non-cavitation conditions in case of tip vortex cavitation (TVC). They have mentioned shift of radiated frequency of maximum amplitude downward from 6.5 kHz at incipient condition to 4 kHz at developed condition. Song et al.<sup>34</sup> have used acoustic approach to determine tip vortex cavitation inception. They only consider overall sound pressure level obtained through frequency spectra and no detailed analysis of nature of spectra is reported. Hosien and Selim<sup>35</sup> carried out acoustic measurements in the range 31.5 Hz to 31.5 kHz using one-third octave band analyser. After analysing sound pressure at various frequency bands they observed that there was a clear and marked increase in pressure level at 4 kHz at the time of inception. Potočník et al.<sup>36</sup> have used extraction of spectral acoustic features for identifying inception of cavitation in valves.

All of the studies reviewed so far were focussed on inception and not on extent of cavitation. In this work, for the first time, we demonstrate a possibility of identifying inception and extent of cavitation by analysis of acoustic signals of vortex based cavitation device acquired using microphones of ordinary mobile phone. Leveraging significant work on audio signal processing and feature extraction (see for example, Sharma et al.<sup>37</sup>), we have used time domain and frequency domain features extracted from acoustic signals to identify the inception and the extent of cavitation. The details of the experimental procedure, data processing and obtained results are discussed in the following. The presented methodology and results will be useful for identification of inception and extent of cavitation in HC devices used in an industrial setting.

## 2. Experiments and acoustic features extraction

The experimental procedure comprised of two parts: i) to construct a cavitation loop to operate the vortex-based cavitation device at different pressure drops ii) to acquire data corresponding to the acoustic signals from the cavitation device. These data were analysed using MATLAB R2020b along with its 'Audio', 'Signal Processing' and 'DSP System' Toolboxes in order to extract several acoustic features. Specific features were further selected in order to decide the relation between inception of cavitation and the pressure drop across the cavitation device. The experimental arrangements, data acquisition and acoustic feature extraction methods are described in the following.

### 2.1 Experimental arrangements and data acquisition

The experimental setup designed for this work was similar to hydrodynamic cavitation device setups used in the literature<sup>10,38,39</sup>. The experimental setup was designed to ensure that cavitation occurred only in the device and not in the pump or valves. A frequency controlled pump (Pedrollo 4 CR 80-n) was used in this setup (see Fig. 1a). The photograph of the actual experimental setup and the devices can be found in previous work<sup>40</sup>. Pre-calibrated analogue pressure gauges procured from Thermosense Direct (P1, downstream of the pump; P2, upstream of the cavitation device and P3, downstream of the cavitation device) in the ranges of 0 – 700 kPa; 0 – 400 kPa and 0 – 100 kPa respectively were used to monitor the pressure. The vortex based cavitation device manufactured in stainless steel was procured from Vivira Process Technologies ([www.vivira.in](http://www.vivira.in)). Further information on the dimensions of the vortex based device used in the study may be found in Simpson and Ranade<sup>24</sup>. Systematic experiments were conducted for vortex based cavitation device with the characteristic throat diameter of 6 mm. Acoustic data was acquired for operating conditions as pressure drop across cavitation device equal to 0, 20, 50, 80, 100, 150, 200, 250, 300, 350 and 390 kPa. Experimental set-ups similar to that described for 6 mm diameter device were used for operating vortex based cavitation devices of throat diameters 3 and 12 mm. Though the internal cavitation device designs for all the three devices (with throat diameters of 3, 6 and 12 mm) were geometrically similar, the actual construction and thickness of device walls were not geometrically similar. The set-ups and devices with 3 mm and 12 mm throat diameter were not designed to suit acquisition of acoustic data as was done with the 6 mm throat diameter device. In order to test the applicability of acquisition and analysis of acoustic signals to any cavitation devices, data were acquired for devices with throat diameters 3 mm and 12 mm as well, at operating pressure drop of 350 kPa.

Initially cavitation noise (for a case with pressure drop across the cavitation device of 250 kPa) was tracked by the means of a stethoscope (Acoustica Deluxe Lightweight Dual Head Stethoscope, MDF

instruments). This stethoscope was used to identify a suitable location on the vortex device (location with ‘maximum intensity’) for monitoring cavitation noise for the range of flow rates/ pressure drop used in this work. It should be noted that the location of collapsing cavities is mainly determined by the pressure recovery in the axial outlet. The pressure field in the HC device and short lifetime of collapsing cavities (less than a millisecond) led to the same measurement location for all the experimental conditions considered in this work. A microphone with the aid of an Android phone (Redmi Note 4) was then used to acquire the cavitation noise data. The position of microphone is shown in Fig. 1b. Operating temperature may influence acoustic signals via changes in sound speed and extent of cavitation. De Giorgi et al.<sup>30</sup> have reported that colder temperatures (20° C) produced more intense noise than warmer temperatures (57° C) for orifice cavitation. Therefore, preliminary experiments were carried out over the operating temperature range of 3 to 45°C. Though it was confirmed that the noise was most intense at coldest temperature (3°C), the key features and extracted inception range was not found to be significantly affected by operating temperature.

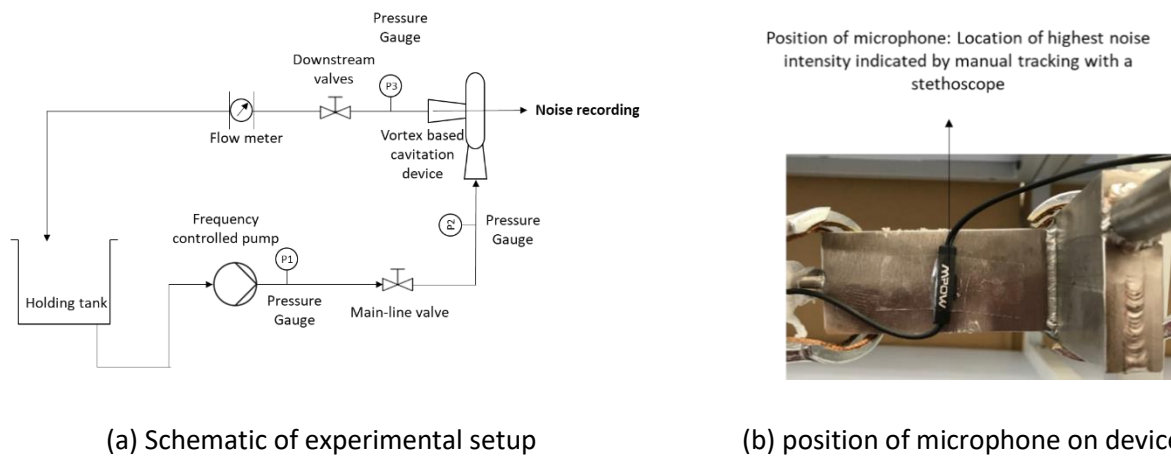


Fig. 1. Experimental set-up.

The relevant frequencies for characterising cavitation noise have been reported as 1 – 44 kHz<sup>7,28,41</sup>. Based on preliminary experiments, data acquisition frequency of 22 kHz was found to be adequate, and was used for subsequent experiments. Different mobile apps for acquiring acoustic signals were evaluated. It was established that the choice of specific app is not critical and any of the apps may be used for data acquisition. The ‘Voice Recorder’ app version 3.0 (downloaded from Playstore: [https://play.google.com/store/apps/details?id=com.media.bestrecorder.audiorecorder&hl=en\\_GB&gl=US](https://play.google.com/store/apps/details?id=com.media.bestrecorder.audiorecorder&hl=en_GB&gl=US)) was used for acquisition in this work. The acquisition of acoustic signals of cavitation was carried out by operating the cavitation device at desired operating condition after allowing flow to stabilise at that operating pressure drop condition. Preliminary analysis of acquired audio signals was carried out to evaluate influence of number of sample points (signal duration) used for feature

extraction. Multiple samples of 2, 4, 8 and 16 s duration were considered. The variation of extracted features within the multiple samples of duration ' $\tau$ ' s was found to be inversely proportional to the considered duration  $\tau$ . These results indicated that the features extracted from audio signals of 16 s duration would have less than 1% variation in multiple samples. Based on this, it was decided to consider audio signal of 20 s duration so that the recording of first and last 2 s duration may be discarded while processing the data to avoid end effects, if any. The acquired data was therefore trimmed to desired duration (20 s) with the help of an online tool, available on [www.mp3cut.net](http://www.mp3cut.net). The trimmed data would contain 441,000 data points of amplitude and time, which served as the raw data for post processing. Recorded raw data was available as '.wav' files, which were used for further processing as discussed in the following section.

## *2.2 Acoustic features extraction*

Acquired acoustic signals were first manually processed by hearing. There was a clear audible indication of cavitation inception showed by an increase in intensity of sound. No pre-processing in the form of filtering was carried out in order to avoid any possibility of losing important frequency components associated with cavitation. A 50 Hz component corresponding to grid frequency was seen to be present in all signals. However, removing that component by using a high pass filter did not influence the values of extracted features. Therefore, all the subsequent analysis was carried out without any filtering. The relevant MATLAB functions used for feature extraction along with their parameters are listed in Table S1 of the supplementary information. A brief description of extracted features is included in the following:

Root-Mean-Square (RMS) Level: gives the measure of average intensity of given signal.

Zero-Crossing Rate (ZCR): It gives the measure of noisiness of a signal.

Spectrogram: gives the strength of different frequencies in the signal with respect to time. Mel scale, which mimics the human ear response and has higher resolution at lower frequency range, was used in this work. A window of 0.03 s corresponding to minimum detected frequency of 33 Hz (lower limit of audibility) was used for calculating the spectrogram (and other time varying features like ZCR). Overlap was set to 0.02 s to compensate for tapering edges of window.

Spectral Centroid: gives the centre of 'gravity' of the spectrum as a function of time. It considers weighted contribution of different frequencies in the spectrum and gives the dominant frequency component which is a representative of the spectrum.

Spectral Crest: gives frequency component with highest strength in the spectrum.

Spectral Flatness: gives uniformity in the strength of different frequency components of the spectrum.

Spectral Spread: is the second central moment of the spectrum indicating spread in the frequency distribution around its mean.

Spectral Skewness: is the third central moment of the spectrum indicating any asymmetry. A perfectly symmetrical spectral distribution has zero skewness. Positive skewness indicates longer tail on higher side of frequency compared to the mean and negative value the opposite.

Spectral Kurtosis: is the fourth central moment of the spectrum indicating the outliers of distribution. Spectral distribution with higher kurtosis indicates many frequency components present away from the major part of frequency distribution.

Spectral Entropy: gives the measure of order in the spectrum and hence increases with noise.

Spectral Slope: is the measure of tendency to have less energy at higher frequencies.

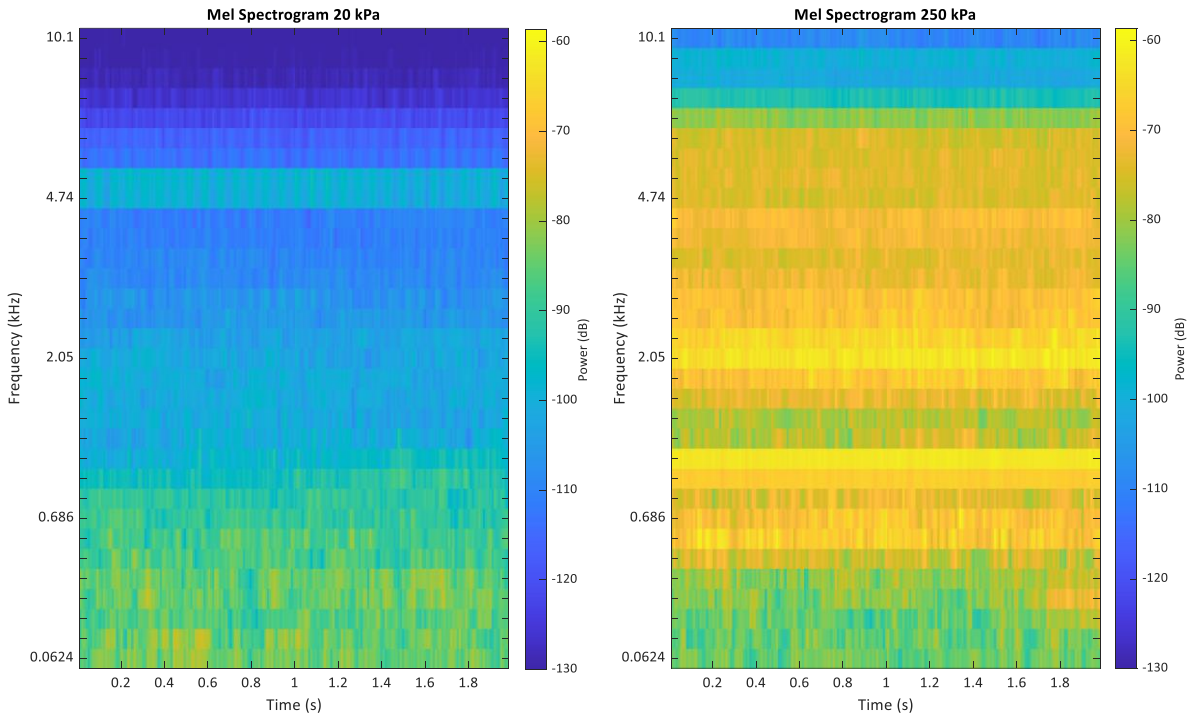
Pitch: gives the fundamental frequency in the signal.

Mel-Frequency Cepstrum Coefficients MFCC-1 to MFCC-13: These coefficients represent the strength of different frequencies (cepstrums) present in the envelope of a log-power spectrum. Such envelopes are characteristics of phonemes or unit of unique sounds. MFCCs are informative and have big classification potential<sup>42</sup>.

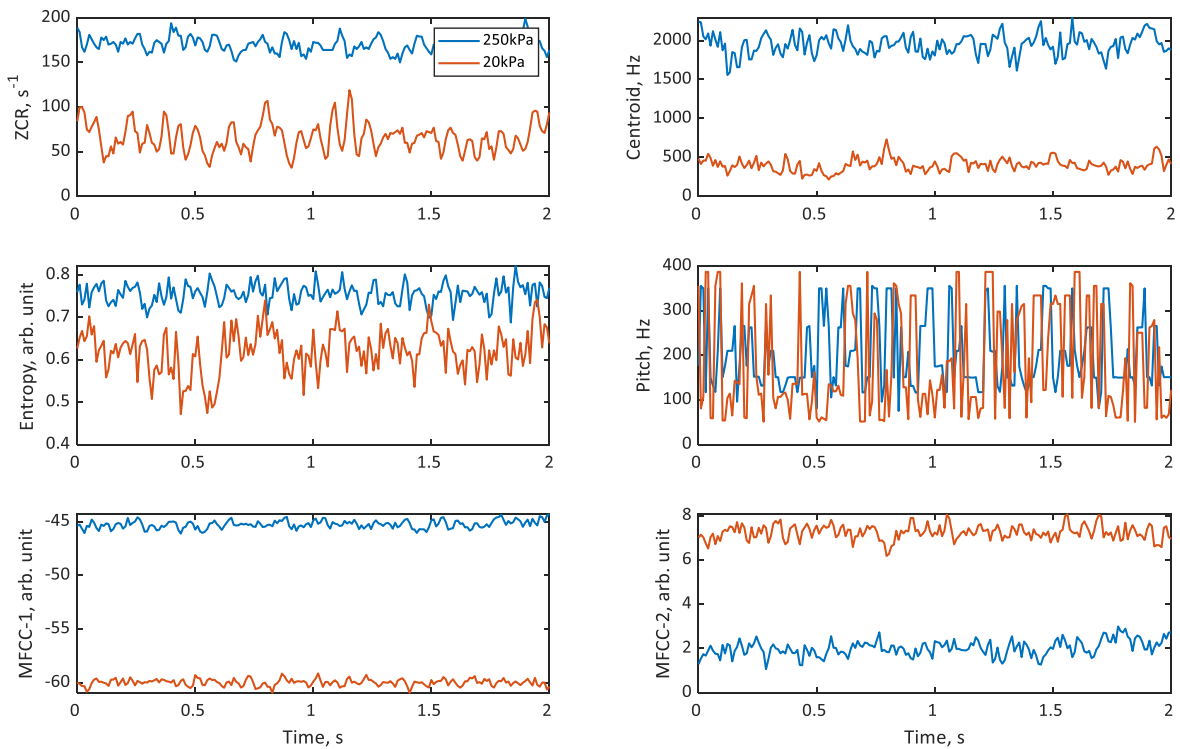
Synchrosqueeze Wavelet Transform: is a time-frequency analysis method that is useful for analysing multicomponent signals with oscillating modes. Its resolution is better than Fourier Transform and it can help detect any mixture of amplitude and frequency modulated signals<sup>43</sup>.

Out of the features listed above, it was essential to identify key features, which capture relevant information about hydrodynamic cavitation. For this purpose, in the first phase, all the features listed above were extracted from acoustic signals acquired for two operating conditions: pressure drop across cavitation as 20 kPa corresponding to a no-cavitation condition and 250 kPa corresponding to a cavitating flow condition. The features, which show distinct variation for these two signals, would carry information about cavitation and were identified as key features. The variation between the two signals was quantified using the two criteria: One criterion was the percentage change in the average value of feature over time. This makes sense as the pressure was maintained constant while recording every signal. Time average of the signal would contain some constant part of the signal influenced by the pressure/ flow. The other was the minimum distance between the two feature signals obtained for these two operating condition as function of time. This would bring out any information in the form of phase of signal that is varying with pressure. The distance was calculated using MATLAB function 'dtw'. Acoustic signals for 20 kPa and 250 kPa were used to extract all the listed 24 features (see Fig. 2 for some of these features).

Mel spectrograms in Fig. 2a of both the signals show frequency on Y-axis with maximum limit set by half of the sampling frequency. The amplitude for every frequency component is colour coded with blue and yellow set to indicate minimum and maximum. The frequency distribution corresponding to the two pressure signals appears to be distinctly different. 250 kPa signal shows dominance of higher frequencies near 700 Hz and from 2000 to 4000 Hz. 20 kPa signal shows dominance of lower frequencies below 600 Hz. The same fact is reflected as seen from the plots of spectral centroid in Fig. 2b. It was observed that RMS value which indicates average amplitude was an order of magnitude higher in case of 250 kPa signal. The ZCR for both signals varied with time with a clear average increase for 250 kPa signal. Spectral entropy differed for the two signals but not considerably whereas pitch appeared to continuously vary within the range 50 to 400 Hz for both the signals. Skewness for 20 kPa was more, indicating asymmetric frequency distribution whereas for 250 kPa it is decreased indicating a more symmetrical spectrum. MFCC-1 also showed a considerable variation. Quantitative comparison of all features for the two signals was carried out by considering the two criteria as percentage difference in their average value and the minimum distance between the feature signals. Since the objective was to choose those features which give clear indication of presence or absence of cavitation, the selected features should have higher percentage change 'AND' higher minimum distance with change in pressure or in cavitation condition. Hence the features were ranked in decreasing order of the product of two criteria. RMS, centroid, spread, ZCR, kurtosis, MFCC-3, pitch, MFCC-11, skewness, MFCC-1, MFCC-2 and MFCC-8 were ranked as topmost 12 features when arranged according to the product of two criteria. The features, pitch and MFCC-11, though ranked higher based on this criterion, were not considered further because of apparent overlap (see Pitch for example in Fig. 2b). Out of the remaining lower 12 features, flatness was shortlisted based on visual inspection. As a result, 10 out of 24 features were shortlisted for studying characteristics of acoustic signals. As mentioned earlier, while processing the trimmed acoustic signals, the recording of first and last 2 s duration was not considered for analysis to avoid end effects, if any. Features were extracted using the acoustic signal of 16 s duration.



(a) Mel spectrograms for 2 s duration from signals corresponding to 20 kPa and 250 kPa.



(b) Few of the extracted features for 2 s duration from signals corresponding to 20 kPa and 250 kPa.

Fig. 2. Comparison of extracted features from 20 and 250 kPa signals.

### 3. Results and discussion

#### 3.1 Pressure dependence of selected features

The short listed 10 features were extracted from acoustic signals acquired for eleven operating conditions (at eleven values of pressure drop across device in the range of 0 to 390 kPa). The variation of these 10 features with respect to pressure drop across cavitation device is shown in Fig. 3.

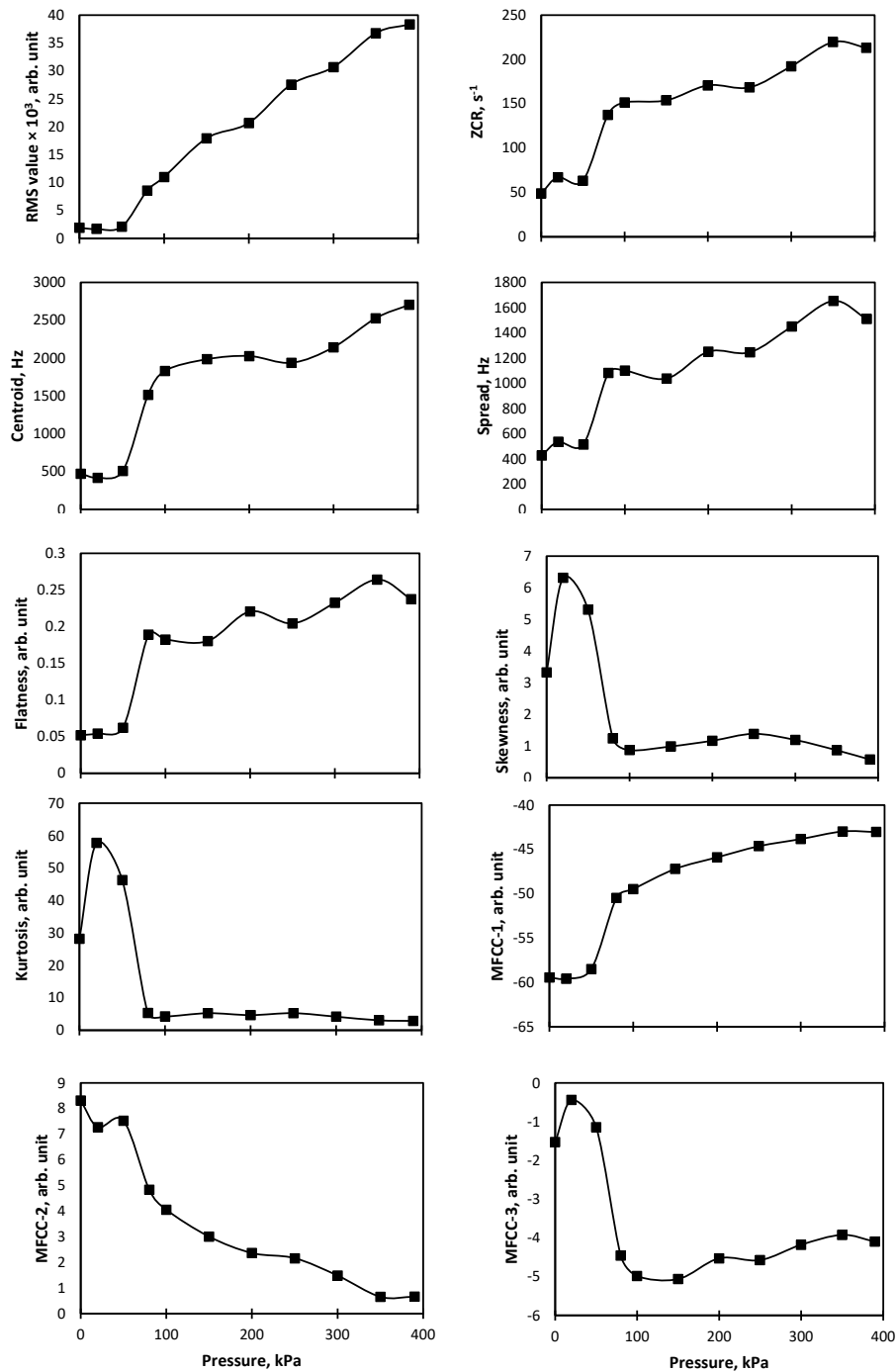


Fig. 3. Influence of pressure drop across device on selected features.

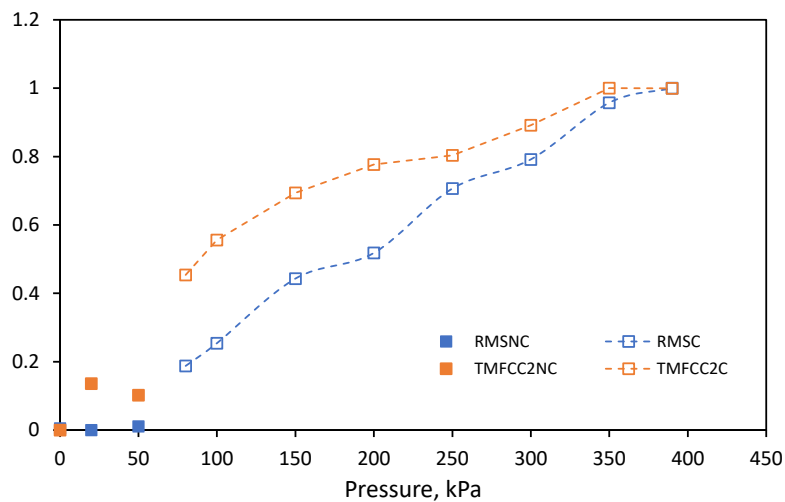
In Fig. 3, feature values (on Y-axis) are plotted versus pressure drop across device in kPa (on X-axis). The RMS value is negligibly small up to 50 kPa and increases at a steady rate till 390 kPa. This indicates a steady increase in the amplitude of audio signal with pressure after 50 kPa. The ZCR is around 50 up to 50 kPa and then shows a step change going to 150 and then remaining more or less constant within the range of 150 to 200 till 390 kPa. This means that there is a step change in the noise level of the audio signal after 50 kPa. The spectral centroid is nearly 500 Hz up to 50 kPa and then shows a step change to 2000 Hz after 50 kPa. Beyond 100 kPa, it remains more or less constant. This indicates that dominant frequencies in audio signals are around 500 Hz up to 50 kPa and show a sudden change to higher frequencies after 50 kPa. The flatness and spread follow same trend as the centroid. This means that after 50 kPa the spectrum appears to have more bandwidth and the strength is more evenly distributed over different frequency components. Skewness has high value (4-6) till 50 kPa and then shows a step change to low value ( $\sim 1$ ). This means that for pressure drop below 50 kPa, frequency distribution is asymmetric. The distribution shifts to a more symmetric one as the pressure drop across cavitation device increases. This appears consistent with the shift in centroid and spread after 50 kPa. Shift in centroid towards higher frequency and simultaneous increase in the spread will make the distribution more symmetric; decreasing the skewness. Kurtosis follows similar trend as skewness. The shift in centroid towards higher frequency and increase in strength of signal beyond 50 kPa is consistent with the observed decrease of kurtosis. Mel frequency cepstrum coefficients (MFCC1, 2 and 3) indicate the strength of different frequencies in the envelop of frequency spectrum. Relatively flat spectrum will have smaller values for these components. MFCC-2 shows a decrease in its value after 50 kPa beyond which the frequency spectrum becomes more flat. MFCC-1 has a negative value which indicates that the first component in the envelop has opposite trend (has a central maximum) to that of a cosine wave. The magnitude of MFCC-1 shows a step decrease beyond 50 kPa. MFCC-3 has a negative value which shows step increase in magnitude with pressure drop beyond 50 kPa. This indicates increased variations in the envelope of frequency spectrum. Thus, it was observed that there was a distinct change in all extracted parameters at pressure value after 50 kPa. Further analysis of their behaviour to decide inception range is carried out in the following section.

### *3.2 Inception range using pressure dependence of selected features*

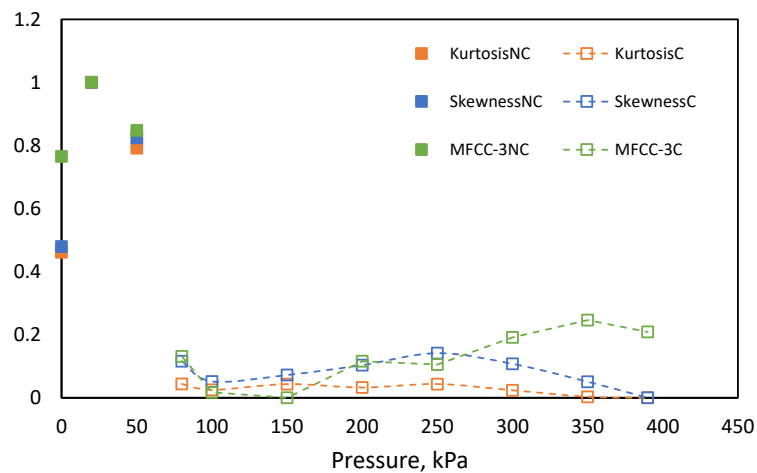
A closer inspection of the ten plots in Fig. 3 indicates that there are three distinct trends in the extracted features with respect to pressure drop across cavitation device. RMS and MFCC-2 show a linear change after 50 kPa. RMS value linearly increases and MFCC-2 linearly decreases. ZCR, spectral centroid, flatness, spread and MFCC-1 show a step increase after 50 kPa followed by a nearly steady value. Spectral skewness, kurtosis and MFCC-3 show initial high value with a step decrease at 50 kPa

followed by negligible change. In order to test the three detected trends due to the similarity in different features, the features were normalized and plotted together. Fig. 4 shows the three plots.

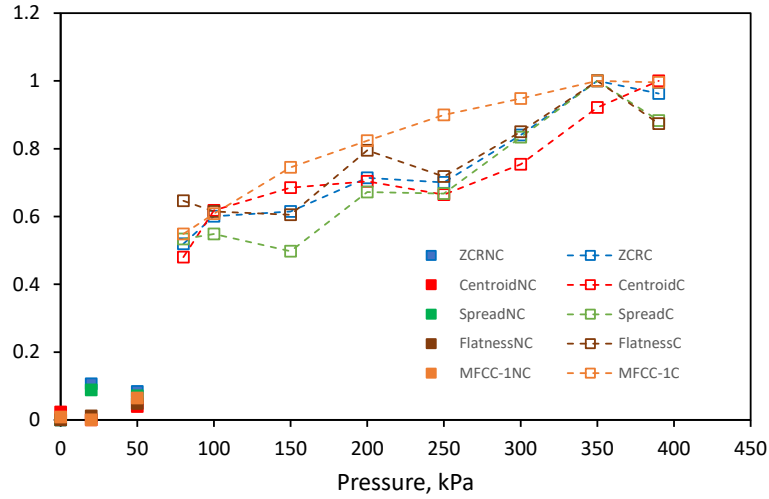
From Fig. 4a, 4b and 4c, it is clear that profiles of normalized features with respect to pressure drop closely follow each other while showing a particular trend. Each plot has two distinct regions; one below 50 kPa having solid markers and the other at and above 80 kPa having open markers (dashed line indicating trend). It was verified by carrying out pollutant degradation experiments that there is clearly absence and presence of cavitation when device is operated at 20 kPa and 250 kPa pressure drop respectively<sup>40</sup>. These two cases distinctly fall in the two different regions whose boundary is somewhere between 50 and 80 kPa as observed from the three plots. Thus, all the extracted features indicate that inception of cavitation in this vortex based cavitation device occurs when pressure drop across the device is somewhere between 50 kPa and 80 kPa.



(a) Normalized RMS and transformed MFCC-2 with pressure.



(b) Normalized Kurtosis, Skewness and MFCC-3 with pressure.



(c) Normalized ZCR, Centroid, Spread, Flatness and MFCC-1 with pressure

Fig. 4. Variation of normalised ( $\phi_N = \frac{\phi - \phi_{min}}{\phi_{max} - \phi_{min}}$ ) extracted features

### 3.3 Extent of cavitation

The extracted features were shown to be useful for identifying inception of cavitation. Apart from identifying inception, it will be instructive to explore whether extracted features from acoustic signals can provide useful information about the extent of cavitation. In order to explore this, influence of operating conditions (pressure drop, flow rate) on extracted features of acoustic signals in the cavitating region is revisited and influence of device scale is briefly discussed.

#### 3.3.1 Influence of operating flow rate/ pressure drop across cavitation device

The preceding sections presented the results based on numerically extracted features from the spectral distribution of acoustic signals. It was also worth carrying out some visual inspection of the spectrogram to note any particular observation missed through the previous analysis. Mel spectrogram used for the previous analysis finds fast fourier transform (FFT) for every window in the spectrogram which is localized in frequency and spread in time. This makes it difficult to detect multicomponent signals with oscillating modes such as amplitude modulated or frequency modulated waves. Wavelet transform decomposes signals by correlating them with different wavelets localized in time and frequency. Hence it brings out oscillating modes in a clearer manner as compared to FFT in the resulting spectrogram. Synchrosqueeze technique further increases the sharpness of spectrum<sup>43</sup>. Considering these aspects, the synchrosqueeze wavelet transform was used for visual observation of spectrogram. Time frames of 0.03 s with an overlap of 0.02 s were used to find synchrosqueeze transform on the scale of 544 different frequencies within the range of 0 – 11 kHz. The spectra for six different signals corresponding to pressures 150 to 390 kPa are shown in Fig. 5.

It can be observed that with increasing pressure, the magnitude of different higher frequency components becomes stronger. It is also possible to mark distinct regions in the spectrum. A small shift in the position of bands along the frequency axis is also apparent. It was also observed that individual band had peculiar variation when zoomed along time axis. It was however difficult to draw any quantitative conclusions based on the observed structures. In order to quantitatively analyse the observations, the spectrograms were averaged over time and frequency spectrum was obtained for each acoustic signal. Such frequency spectra for acoustic signals corresponding to different pressure drops across cavitation device are shown in Fig. 6a.

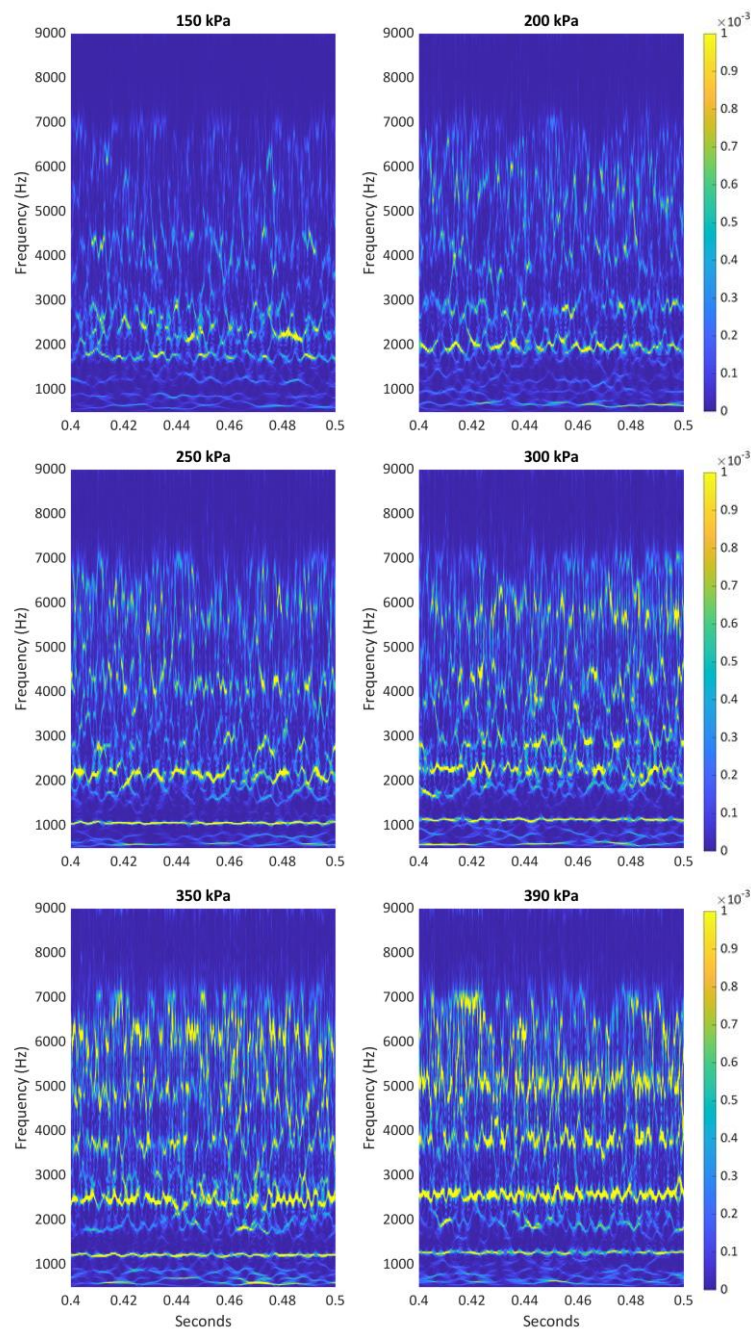
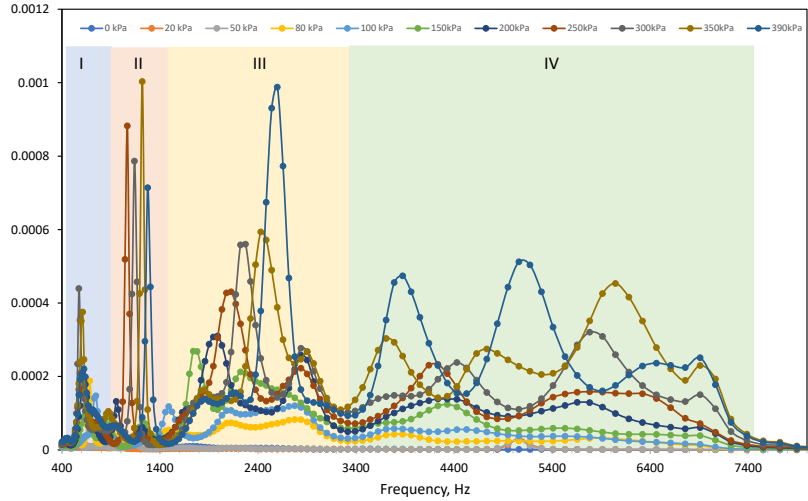
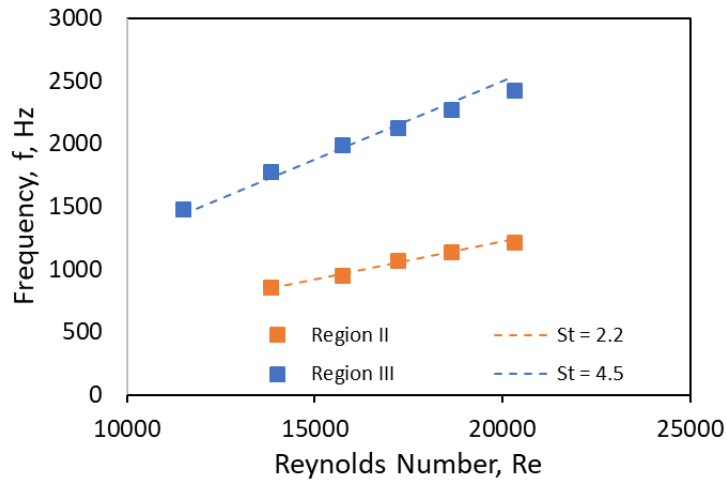


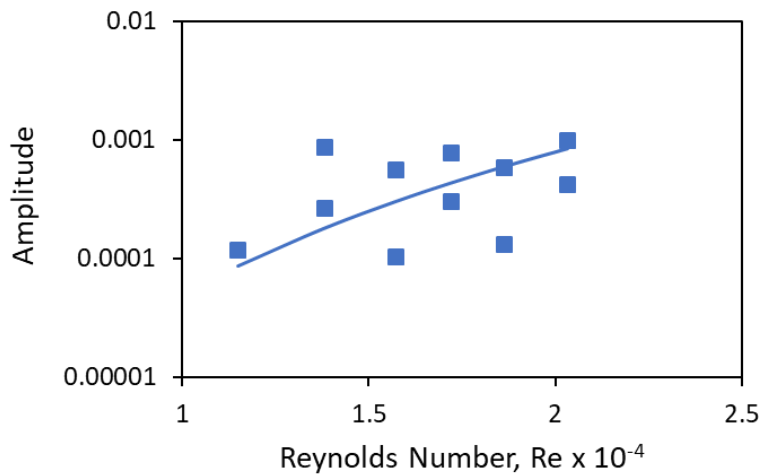
Fig. 5. Synchrosqueeze wavelet transforms for signals at different pressures.



(a) Superimposed time averaged spectra at different pressure drop across cavitation device



(b) Shift of peak frequencies with Reynolds number ( $St = \text{Strouhal number} = \frac{f d_t}{V_t}$ )



(c) Variation of peak-strength with Reynolds number

Fig. 6. Influence of Reynolds number ( $Re = \frac{d_t V_t \rho}{\mu}$ ) / Pressure drop across cavitation device.

Four regions could be identified on the x-axis depending on the prominent peaks at different frequencies (indicated by different background colour). Signals corresponding to pressure 80 kPa and above have at least one prominent peak in each of the four regions. Region I and II have one peak whereas region III and IV have two and three peaks respectively for each pressure drop value within the range 80 to 390 kPa. As a result, regions III and IV are wider compared to I and II. Considering the range, mean value of frequency for the four regions turns out to be 592, 1206, 2281 and 5170 Hz respectively. The frequencies for regions II, III and IV may be considered as the 2<sup>nd</sup>, 3<sup>rd</sup> and 4<sup>th</sup> harmonics of the frequency representing region I. A close observation of peaks in region II and III indicates that the peak frequencies have a shift with increase in pressure drop across cavitation device. The observed shift in frequencies is shown in Fig. 6b for regions II and III. The dashed lines in Fig. 6b indicate lines of constant values of Strouhal number ( $St = \frac{f d_t}{V_t}$ ). The higher value of Strouhal number indicates that oscillations dominate the flow. The Strouhal number for the region II was found to be 2.2. The Strouhal number for region III was found to be approximately double of that found for Region II. This is consistent with the observed harmonics. The amplitude of the observed peaks is found to scale with the fourth power of Reynolds number,  $Re^4$  (as can be seen from Fig. 6c) which is consistent with the intuitive understanding.

The variation of key extracted features with operating conditions (pressure drop/ flow rate) shown in Fig. 4 exhibit specific trends with respect to operating conditions and have a potential to provide a pathway to estimate extent of cavitation.

### 3.3.2 Influence of device scale

In order to investigate the role of acoustic features in capturing the effect of scale on cavitation in vortex based devices, similar data was acquired for the devices with throat diameters equal to 3 mm and 12 mm. The acoustic signals were analysed in similar way to extract all features. The features extracted from acoustic signals for an operating case with pressure drop across cavitation devices as 350 kPa are shown in Fig. 7 for three scales of devices (throat diameters of 3 mm, 6 mm and 12 mm). It can be seen that the values of ZCR, flatness and spread consistently decrease with increase in scale; whereas the values of skewness and kurtosis increase with increase in scale. It is interesting to note that all these features show almost the same trend when examined after appropriate normalisation. This fact indicates that acoustic features are able to capture the effect of scale on cavitation in some manner. In order to examine a quantitative relation, one of these features, flatness was selected. Variation of flatness with respect to scale of the cavitation device (characterised by the throat

diameter) is shown in Fig. 8. It can be seen that flatness exhibits linear relationship with the inverse of throat diameter.

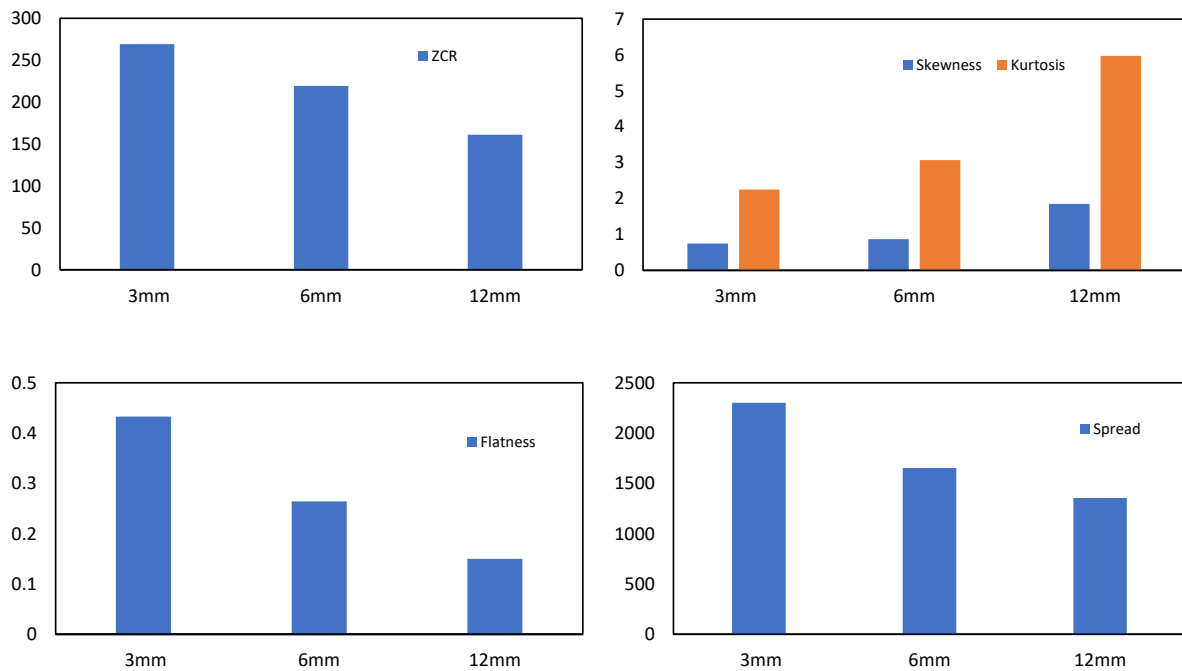


Fig. 7. Comparison of different features at 350 kPa for 3 different scales.

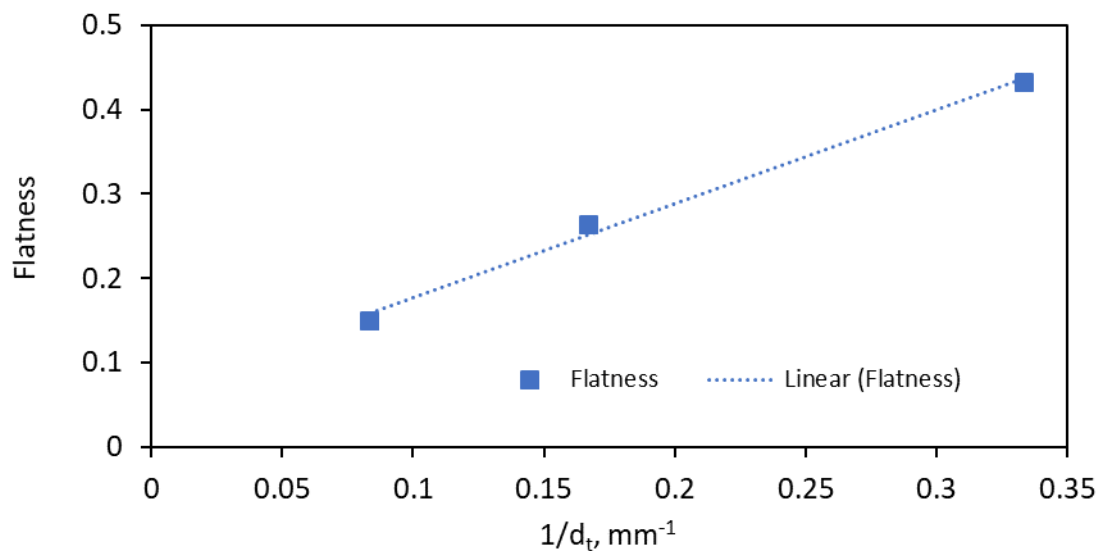


Fig. 8. Flatness at 350 kPa as a function of inverse of throat diameter.

### 3.3.3 Relating features of acoustic signals with extent of cavitation or device performance

In a recent study, Ranade et al.<sup>2</sup> have reported performance of vortex based cavitation devices for degrading organic pollutant [2,4 dichloroaniline (DCA)] in water for a range of pressure drops (for one device) and for a range of device scales (for one pressure drop). Here, an attempt is made to examine

relationships between features extracted from acoustic signals and device performance. The HC device performance is quantified by its ability to degrade DCA in a single-pass through the cavitation device (per-pass degradation factor or per-pass performance factor).

A scrutiny of experimentally observed performance of HC devices over the reported range of parameters (pressure drop and device scale) reveals that the relative variation of per-pass device performance with respect to pressure drop for a given scale of device is much smaller compared to the variation in device performance with respect to device scale. As a first step, it was therefore decided to mainly explore relationship between features of acoustic signals with device performance as a function of scale and assume more or less same performance for a given scale of device across all flow rates/ pressure drops. This obviously is an approximation. It is however worthy to examine such a possibility since it will open up a promising avenue to gauge performance of a hydrodynamic cavitation device by simply analysing acoustic signals acquired using normal mobile phone.

Examination of Fig. 8 indicates that 'Flatness' decreases as scale increases and it exhibits some kind of limiting value at infinite scale ( $F_\infty$  is value of flatness as  $\frac{1}{d_t} \rightarrow 0$ ). Ranade et al.<sup>2</sup> have observed that the performance of the vortex based cavitation devices also decreases as scale increases (at constant pressure drop across all considered scales). They have observed the following relationship between the per-pass performance factor with scale as:

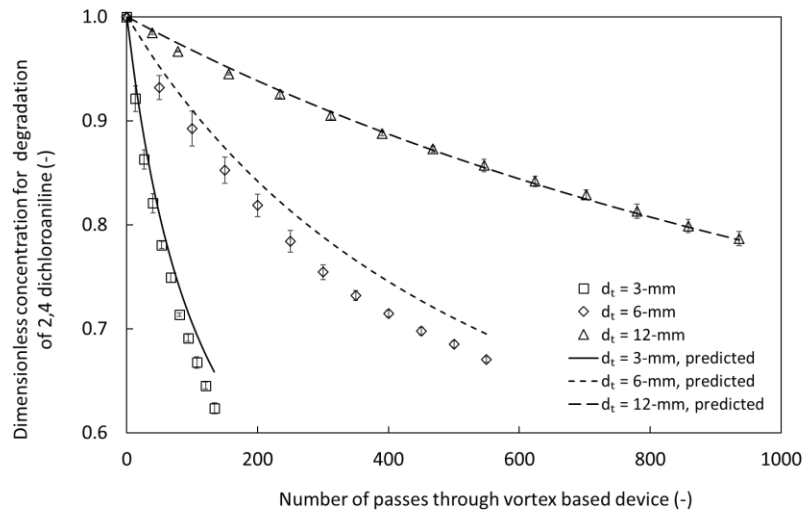
$$\phi_0 = \phi_\infty e^{10.85/d_t} \quad (1)$$

By comparing the variation of flatness and per pass performance factor with scale, it may be possible to eliminate device scale and relate per-pass performance factor with flatness as:

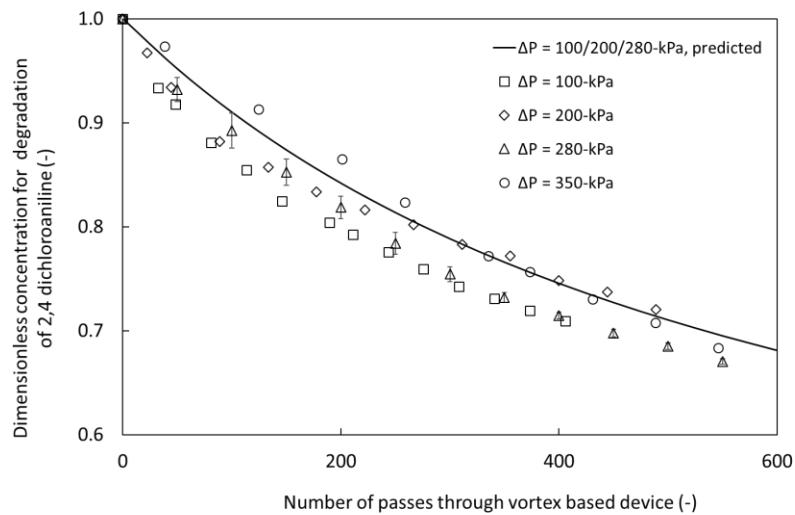
$$\ln\left(\frac{\phi_0}{\phi_\infty}\right) \propto \left(\frac{F}{F_\infty} - 1\right) \quad (2)$$

Ranade et al.<sup>2</sup> have reported the value of  $\phi_\infty$  as  $1.5 \times 10^{-4}$ . The value of  $F_\infty$  was found to be 0.0657 (Fig. 8). The proportionality constant for the Equation (2) was found to be 0.64. Using these values of parameters appearing in Equation (2), per-pass performance factor was estimated. The profiles of dimensionless concentration of DCA as a function of number of passes through cavitation device were then predicted following the model of Ranade et al.<sup>2</sup>. The predicted profiles are compared with the experimental data of Ranade et al.<sup>2</sup> in Fig. 9. It can be seen from Fig. 9a that the per-pass performance factor estimated using the value of 'flatness' extracted from the acoustic signal and Equation (2) could

capture the influence of scale on performance of cavitation device in terms of DCA degradation quite well. Assuming the same per-pass performance factor, dimensionless profiles of DCA concentrations at different pressure drop across cavitation device with 6 mm throat diameter are shown in Fig. 9b which again shows reasonably good agreement with experimental data.



(a) Influence of scale (3, 6 and 12 mm devices)



(b) Influence of pressure drop (6 mm device)

Fig. 9: Comparison of results predicted using ‘flatness’ extracted from acoustic signals and Equation (2) with the experimental data of Ranade et al.<sup>2</sup>.

The agreement between experimental data and results predicted using features of acoustic signals and Equation (2) are quite encouraging. The Equation (2) and the proposed relationship between

flatness and per-pass performance factor appears to be rather speculative at the moment. The point is not to emphasise the specific nature of this equation. The key message is that for the first time, it looks feasible to establish a relationship between features of acoustic signals and per-pass performance factors of cavitation device. Further work is needed to develop better understanding of such relationships. Ranade et al.<sup>44</sup> have developed artificial neural network (ANN) model to relate dimensionless concentration profiles of DCA with number of passes, device scale and pressure drop across devices. Similar approach may be used to develop quantitative relationship between number of passes and couple of features extracted from acoustic signals with per-pass performance of cavitation devices. The features like 'flatness' (to capture influence of scale) and the second feature like say 'skewness' (to capture influence of pressure drop/ Reynolds number) on device performance may be used for developing such ANN based model. Further work on simultaneous measurement of acoustic data and cavitation device performance is needed to validate the key trends presented in this work. Such additional data, application of methods of feature extraction discussed in this work and ANN based approach (like Ranade et al.<sup>44</sup>) may be used to develop an effective and simple on-line tool for quantifying device performance. Such a tool when developed will be very useful for design, optimisation and scale-up of cavitation based processes.

#### **4. Summary and conclusion**

A simple, non-invasive method based on analysis of acoustic signals was developed to characterise inception and extent of cavitation. The methodology was applied for processing acoustic signals acquired from three vortex based cavitation devices (with throat diameters of 3, 6 and 12 mm). An attempt was made to relate features extracted from acoustic signals to per-pass performance of cavitation devices. The key conclusions from the study are as follows:

- Temperature did not significantly influence the cavitation inception range of vortex based cavitation devices (up to 45 °C).
- Ten key features extracted from acoustic signals exhibited three distinct trends with respect to pressure drop across cavitation devices. All the three trends were able to clearly distinguish between non-cavitating and cavitating conditions.
- All the three trends predicted the cavitation inception between 50 to 80 kPa for the vortex based cavitation device used in this work.
- Time averaged spectrogram at different pressure values showed distinct shift of peak frequencies and increase in amplitude of peaks in a specific region of spectra. The signal exhibited distinct harmonics. The Strouhal number was found to be multiples of 2.2. The amplitude of the peaks was found to scale with  $Re^4$ .

- Features extracted for acoustic signals captured the influence of device scale (represented by the throat diameter).
- It was feasible to estimate per-pass performance of cavitation devices using an empirical relationship with features extracted from acoustic signals. This was demonstrated using ‘flatness’ as a characteristic feature for capturing influence of device scale.

The methodology and results presented in this work demonstrate feasibility of developing a simple, non-invasive tool for identifying inception and extent of hydrodynamic cavitation that is suitable to industrial setting. The results obtained so far are encouraging and point out an interesting possibility towards developing ANN based tool for on-line detection of per-pass performance of cavitation using acoustic signals.

### Acknowledgements

The authors gratefully acknowledge funding support from the Leverhulme Trust (RPG-2019-127) for carrying out part of this research.

### Notations

$d_t$	Diameter of throat of cavitation device (mm)
$f$	Frequency, Hz
$F$	Flatness
$\Delta P$	Pressure drop across cavitation device (kPa)
$Re$	Reynolds number $(\frac{d_t V_t \rho}{\mu})$
$St$	Strouhal number $(\frac{f d_t}{V_t})$
$T$	Bulk temperature, (K)
$V_t$	Velocity at throat of cavitation device (m/s)
$\phi$	Per-pass performance factor (-)
$\phi_o$	Initial per-pass performance factor (-)
$\mu$	Viscosity, Pa.s
$\rho$	Density, kg/m <sup>3</sup>

## References

1. Suryawanshi, P.G.; Bhandari, V.M.; Sorokhaibam, L.G.; Ruparelia, J.P.; Ranade, V.V. Solvent degradation studies using hydrodynamic cavitation. *Environ. Prog. Sustainable Energy*. **2018**, *37*, 295-304.
2. Ranade, V.V.; Sarvothaman, V.P.; Simpson, A.; Nagarajan, S.; Group, I. Scale-up of vortex based hydrodynamic cavitation devices: A case of degradation of di-chloro aniline in water. *Ultrason. Sonochem.* **2021**, *70*, 105295.
3. Farvardin, M.; Hosseinzadeh Samani, B.; Rostami, S.; Abbaszadeh-Mayvan, A.; Najafi, G.; Fayyazi, E. Enhancement of biodiesel production from waste cooking oil: ultrasonic-hydrodynamic combined cavitation system. *Energy Sources, Part A*, **2019**, 1-15.
4. Nagarajan, S.; Ranade, V.V. Pre-treatment of distillery spent wash (vinasse) with vortex based cavitation and its influence on biogas generation. *Bioresour. Technol.* **2020**, *11*, 100480.
5. Holkar, C.R.; Jadhav, A.J.; Pinjari, D.V.; Pandit, A.B. Cavitationally driven transformations: A technique of process intensification. *Ind. Eng. Chem. Res.* **2019**, *58*, 5797-5819.
6. Mancuso, G.; Langone, M.; Andreottola, G. A critical review of the current technologies in wastewater treatment plants by using hydrodynamic cavitation process: principles and applications. *J. Environ. Health Sci. Eng.* **2020**, *18*, 311-333.
7. Brennen, C.E. *Cavitation and bubble dynamics*. Cambridge University Press, 2014.
8. Sawant, S.S.; Anil, A.C.; Krishnamurthy, V.; Gaonkar, C.; Kolwalkar, J.; Khandeparker, L.; Desai, D.; Mahulkar, A.V.; Ranade, V.V.; Pandit, A.B. Effect of hydrodynamic cavitation on zooplankton: a tool for disinfection. *Biochem. Eng. J.* **2008**, *42*, 320-328.
9. Pandit, A.; Sarvothaman, V.; Ranade, V.V. Estimation of Chemical and Physical Effects of Cavitation by Analysis of Cavitating Single Bubble Dynamics, *Ultrason. Sonochem.* revised version under review.
10. Soyama, H.; Hoshino, J. Enhancing the aggressive intensity of hydrodynamic cavitation through a Venturi tube by increasing the pressure in the region where the bubbles collapse. *AIP Adv.* **2016**, *6*, 045113.
11. Pawar, S.K.; Mahulkar, A.V.; Pandit, A.B.; Roy, K.; Moholkar, V.S. Sonochemical effect induced by hydrodynamic cavitation: Comparison of venturi/orifice flow geometries. *AIChE J.* **2017**, *63*, 4705-4716.
12. Thoroddsen, S.T.; Etoh, T.G.; Takehara, K. High-speed imaging of drops and bubbles. *Annu. Rev. Fluid Mech.* **2008**, *40*, 257-285.
13. Goldstein, R. *Fluid mechanics measurements*. Routledge, 2017.
14. Adrian, L.; Adrian, R.J.; Westerweel, J. *Particle image velocimetry*. Cambridge university press, 2011.
15. Iida, Y.; Yasui, K.; Tuziuti, T.; Sivakumar, M. Sonochemistry and its dosimetry. *Microchem. J.* **2005**, *80*(2), 159-164.
16. Sutkar, V.S.; Gogate, P.R. Design aspects of sonochemical reactors: techniques for understanding cavitation activity distribution and effect of operating parameters. *Chem. Eng. J.* **2009**, *155*, 26-36.
17. De-Nasri, S.J.; Nagarajan, S.; Robertson, P.K.; Ranade, V.V. Quantification of hydroxyl radicals in photocatalysis and acoustic cavitation: Utility of coumarin as a chemical probe. *Chem. Eng. J.*, **2020**, 127560.
18. Arakeri, V.H. Cavitation inception. *Proceedings of the Indian Academy of Sciences Section C: Engineering Sciences*, **1979**, *2*, 149-177.
19. Rood, E.P. Mechanisms of cavitation inception, *J. Fluids Eng.* **1991**, *113*, 163-175.
20. Sakamoto, N. and Kamiirisa, H., 2018. Prediction of near field propeller cavitation noise by viscous CFD with semi-empirical approach and its validation in model and full scale. *Ocean Eng.*, **168**, 41-59.

21. Quan, K.M.; Avvaru, B.; Pandit, A.B. Measurement and interpretation of cavitation noise in a hybrid hydrodynamic cavitating device. *AIChE J.* **2011**, 57(4), 861-871.
22. Mancuso, G. Experimental and numerical investigation on performance of a swirling jet reactor. *Ultrason. Sonochem.* **2018**, 49, 241-248.
23. Peng, X.X.; Zhang, L.X.; Wang, B.L.; Xu, L.H.; Song, M.T.; Cao, Y.T.; Liu, Y.W.; Hong, F.W.; Yan, K. Study of tip vortex cavitation inception and vortex singing. *J Hydrodyn*, **2019**, 31(6), 1170-1177.
24. Simpson, A.; Ranade, V.V. 110th Anniversary: Comparison of Cavitation Devices Based on Linear and Swirling Flows: Hydrodynamic Characteristics. *Ind. Eng. Chem. Res.* **2019**, 14488-14509.
25. Ceccio, S.L.; Mäkiharju, S.A. Experimental methods for the study of hydrodynamic cavitation. *In Cavitation Instabilities and Rotordynamic Effects in Turbopumps and Hydroturbines*, **2017**, 35-64.
26. De, M.K.; Hammitt, F.G. New method for monitoring and correlating cavitation noise to erosion capability. **1982**.
27. He, Y.; Liu, Y. Experimental research into time–frequency characteristics of cavitation noise using wavelet scalogram. *Appl. Acoust.* **2011**, 72(10), 721-731.
28. Gaikwad, V.D. Water disinfection using hydrodynamic cavitation, **2016**, Ph.D. Thesis, CSIR-National Chemical Laboratory, Pune.
29. Avvaru, B.; Pandit, A.B. Oscillating bubble concentration and its size distribution using acoustic emission spectra. *Ultrason. Sonochem.* **2009**, 16(1), 105-115.
30. De Giorgi, M.G.; Ficarella, A.; Tarantino, M. Evaluating cavitation regimes in an internal orifice at different temperatures using frequency analysis and visualization. *Int. J. Heat Fluid Flow*, **2013**, 39, 160-172.
31. Wang, J.; Cheng, H.; Xu, S.; Ji, B.; Long, X. Performance of cavitation flow and its induced noise of different jet pump cavitation reactors. *Ultrason. Sonochem.* **2019**, 55, 322-331.
32. Tabrizi, A. B.; Wu, B. Noise investigation of a cavitating orifice: use of cfd simulation and fflowcs williams–hawkins (fw-h) formulation to gain insight into acoustics condition. *IOP Conference Series: Earth and Environmental Science.* **2018**, 163, 012087.
33. Park, J., Seong, W. Experimental study on the effect of number of bubble occurrences on tip vortex cavitation noise scaling law. *J. Fluids Eng.* **2017**, 139.
34. Song, M.; Xu, L.; Peng, X.; Tang, D. An acoustic approach to determine tip vortex cavitation inception for an elliptical hydrofoil considering nuclei-seeding. *Int. J. Multiphase Flow*, **2017**, 90, 79-87.
35. Hosien, M. A.; Selim, S. M. Acoustic detection of cavitation inception. *Journal of J. Appl. Fluid Mech.* **2017**, 10, 31-40.
36. Potočník, P.; Olmos, B.; Vodopivec, L.; Susič, E.; Govekar, E. Condition classification of heating systems valves based on acoustic features and machine learning. *Appl. Acoust.* **2021**, 174, 107736.
37. Sharma, G.; Umapathy, K.; Krishnan, S. Trends in audio signal feature extraction methods. *Appl. Acoust.* **2020**, 158, 107020.
38. Saharan, V. K.; Pinjari, D. V.; Gogate, P. R.; Pandit, A. B. Advanced Oxidation Technologies for Wastewater Treatment: An Overview. In *Industrial Wastewater Treatment, Recycling and Reuse*; Ranade, V.; Bhandari, V. M. Eds.; Elsevier: 2014, 141–191.
39. Sarvothaman, V.P.; Nagarajan, S.; Ranade, V.V. Treatment of solvent-contaminated water using vortex-based cavitation: influence of operating pressure drop, temperature, aeration, and reactor scale. *Ind. Eng. Chem. Res.* **2018**, 57, 9292-9304.
40. Sarvothaman, V. P. Hydrodynamic Cavitation for Effluent Treatment: Using Vortex-Based Cavitation Devices. **2020**, Ph.D. Thesis, Queen’s University Belfast.
41. Martin, C.S.; Medlarz, H.; Wiggert, D.C.; Brennen, C. Cavitation inception in spool valves. *J. Fluids Eng.* **1981**, 103, 564-575.

42. Liu, X.; Pei, D.; Lodewijks, G.; Zhao, Z.; Mei, J. Acoustic signal based fault detection on belt conveyor idlers using machine learning. *Adv. Powder Technol.* **2020**, 31(7), 2689-2698.
43. Daubechies, I.; Lu, J.; Wu, H. T. Synchrosqueezed wavelet transforms: An empirical mode decomposition-like tool. *Appl. Comput Harmon A.* **2011**, 30(2), 243-261.
44. Ranade, N.V.; Nagarajan, S.; Sarvothaman, V.; Ranade, V.V. ANN based modelling of hydrodynamic cavitation processes: Biomass pre-treatment and wastewater treatment. *Ultrason. Sonochem.* **2021**, 72, 105428.